Theor Chem Acc (2001) 106: 241–250
DOI 10.1007/s002140100271

Theoretical
Chemistry Accounts

*Regular article*

# Calculations of the geometries, electronic structures and nonlinear second-order optical susceptibilities of spiroannelated quinone-type methanofullerenes

**Wei Fu, Ji-Kang Feng, Ge-Bo Pan, Xiang Zhang**

State Key Laboratory of Theoretical and Computational Chemistry, Institute of Theoretical Chemistry, Jilin University, Changchun 130023, China

Received: 17 December 2000 / Accepted: 16 March 2001 / Published online: 13 June 2001


**Abstract.** The equilibrium geometries, electronic structures and UV–vis spectra of a series of spiroannelated quinone-type methanofullerenes have been determined by using Zerner's intermediate neglect of differential overlap method. The results show that between fullerene and the addend there exists a special interaction, "periconjugation", which results in through-space orbital interactions. The calculated UV–vis spectra are in good agreement with experiments. On the basis of the electronic spectra, the $\beta$ values are calculated. The results show that spiroannelated quinone-type methanofullerenes have quite large $\beta$ values. We attribute the large $\beta$ values to both the charge transfer from $C_{60}$ to benzoquinone and on the $C_{60}$ three-dimensional conjugated sphere.

**Key words:** Spiroannelated quinone-type methanofullerenes – Geometry – UV–vis spectra – Nonlinear second-order susceptibilities

## 1 Introduction

Since $C_{60}$ was first discovered [1], it has generated great interest for both theoretical predictions [2–4] and experimental observations [5, 6], owing to its symmetrical sphere, large size and properties of the $\pi$-conjugated system. We have successfully examined the electronic spectrum and nonlinear third-order susceptibility [$<\gamma>(-\omega;\omega, -\omega, \omega) = 7.30 \times 10^{-34}$ esu, $\omega = 1.064$ $\mu$m] of $C_{60}$ [4], which showed good agreement with experiment. Obviously, the second-order optical susceptibility, $\beta$, is zero for $C_{60}$ owing to its centrosymmetric structure. However, by forming chemically modified fullerene, its center of symmetry is broken and the second-order optical nonlinearity is induced. Recent research has focused on the chemically modified fullerenes whose nonlinear optical (NLO) properties have been studied both theoretically and experimentally [7, 8]. We have previously reported theoretical studies on the different $C_{60}$/donor systems, such as $C_{60}$/aniline [7], $C_{60}$/ferrocene [9], $C_{60}$/Tetrathiafulvalene (TTF) [10] and so on, which showed that the $C_{60}$ derivatives have quite large second-order nonlinear responses. The calculations of some molecules have reproduced the experimental results. Recently, a series of spiroannelated quinone-type methanofullerenes have been prepared in several experiments [11–13], but few theoretical studies on the nonlinear second-order susceptibility of these compounds have been reported. In order to obtain the equilibrium geometries, to study the second-order optical nonlinearity and to explore the source of the NLO response for these compounds (Fig. 1), semiempirical intermediate neglect of differential overalap (INDO) calculations were carried out. Firstly, the electronic structures and UV–vis spectra were determined using Zerner's INDO (ZINDO) [14] method. The results are consistent with those of the experiments. Secondly, the second-order optical susceptibility was calculated using the ZINDO–sum-over-states (SOS) expression on the basis of the electronic spectra. The calculated $\beta$ values are relatively large.

## 2 Theoretical methods

A quantitative description of molecular NLO response is derived from a power-series expansion of the molecular polarization upon interaction with an oscillating external electromagnetic field (Eq. 1).

$$P_i = \sum_j \alpha_{ij} E_j + \sum_{j\geq k} \beta_{ijk} E_j E_k + \sum_{j\geq k\geq l} \gamma_{ijkl} E_j E_k E_l + \cdots\cdots \quad (1)$$

Here $P_i$ is the molecular polarization induced along the $i$th axis, $E_j$ is the $j$th component of the applied electric field, $\alpha$ is the linear polarizability, $\beta$ is the first hyperpolarizability or the second-order susceptibility and $\gamma$ is the second hyperpolarizability or the third-order susceptibility. $\alpha$, $\beta$ and $\gamma$ describe the responsivity of the molecule to an electromagnetic perturbation and are constants for

*Correspondence to*: J.-K. Feng

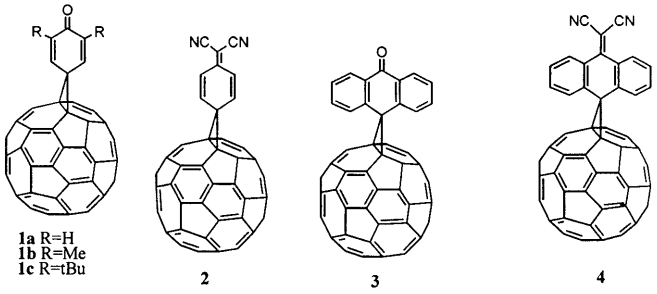


**Fig. 1.** Spiroannelated quinone-type methanofullerenes

a given molecular geometry and external electromagnetic field. $\beta$ and $\gamma$ are responsible for second-harmonic and third-harmonic generation. The SOS expression for the individual components of the second-order susceptibility tensor has been given from perturbation theory [15, 16]:

$$\begin{aligned}\beta_{ijk}+\beta_{ijk}=\frac{1}{4\hbar^2}\Bigg\{\sum_{\substack{n\neq n'\\ n\neq g\\ n\neq g}}\Bigg[&\left(r^j_{gn'}r^i_{n'n}+r^k_{gn}+r^k_{gn'}r^i_{n'n}r^j_{gn}\right)\\ &\times\left(\frac{1}{(\omega_{n'g}-\omega)(\omega_{ng}+\omega)}+\frac{1}{(\omega_{n'g}+\omega)(\omega_{ng}-\omega)}\right)\\ &+\left(r^i_{gn'}r^j_{n'n}r^k_{gn}+r^i_{gn'}r^k_{n'n}r^j_{gn}\right)\\ &\times\left(\frac{1}{(\omega_{n'g}-2\omega)(\omega_{ng}-\omega)}+\frac{1}{(\omega_{n'g}+2\omega)(\omega_{ng}+\omega)}\right)\\ &+\left(r^j_{gn'}r^k_{n'n}r^i_{gn}+r^k_{gn'}r^j_{n'n}r^i_{gn}\right)\\ &\times\left(\frac{1}{(\omega_{n'g}-\omega)(\omega_{ng}-2\omega)}+\frac{1}{(\omega_{n'g}+\omega)(\omega_{ng}+2\omega)}\right)\\ &+4\sum_n\Bigg\{\Big[r^j_{gn}r^k_{gn}\Delta r^i_n\left(\omega^2_{ng}-4\omega^2\right)\\ &+r^i_{gn}\left(r^k_{gn}\Delta r^j_n+r^j_{gn}\Delta r^k_n\right)\left(\omega^2_{ng}+2\omega^2\right)\Big]\\ &\times\left(\frac{1}{\left(\omega^2_{ng}-\omega^2\right)\left(\omega^2_{ng}-4\omega^2\right)}\right)\Bigg\}\Bigg\}\ ,\end{aligned}\tag{2}$$

where the summations are over the complete sets of eigenstates $|n>$ and $|n'>$ of the unperturbed molecular system. The quantities $r^i_{gn'}$ and $r^i_{nn'}$ are matrix elements of the $i$th components of the dipole operator between the unperturbed ground and excited states and between the two excited states, respectively; $\Delta r^i_n = r^i_{nn}-r^i_{gg}$ is the difference between the excited-state and ground-state energies. Although all 27 components of the $\beta$ tensor can be computed, only the vector component in the dipolar direction ($\beta_\mu$) is sampled by electric-field-induced second harmonic generation (EFISH) experiments. $\beta_\mu$ is given by

$$\beta_\mu=(\mu_x\beta_x+\mu_y\beta_y+\mu_z\beta_z)/(\mu_{x^2}+\mu_{y^2}+\mu_{z^2})^{1/2}\ ,\tag{3}$$

where

$$\beta_i=\beta_{iii}+1/3\sum_{i\neq j}\beta_{jii}+\beta_{iji}+\beta_{iij})\ i,j\in(x,y,z)\ .\tag{4}$$

The all-valence ZINDO technique [14] was employed to provide the transition dipole moment and the transition energy needed in the SOS expressions (Eq. 2). Standard parameters and basis functions were used. The ZINDO–SOS method is of proven reliability in the description of molecular NLO properties [17, 18]. The second-order susceptibilities [7, 19, 20] and the third-order susceptibilities [4, 21, 22] of dozens of molecules have been reported in our previous work. In the present approach, the single-determinant and molecular orbital (MO) approximate ground state was used, and the monoexcited configuration interaction (MECI) approximation was employed to describe the excited states. In computation of a series of quinone-type fullerenes, the 290 lowest-energy transitions between self-consistent field and MECI electronic configurations were chosen to undergo CI mixing. The 290 states were found to be sufficient for effective convergence of the SOS procedure.

## 3 Results and discussion

### *3.1 Geometry structure*

Using the INDO/2 method (included in the ZINDO package), the geometries of spiroannelated quinone-type methanofullerenes were optimized. With the same method we have previously obtained the equilibrium geometry of $C_{60}$, where $R_{6-6}=1.3979$ Å and $R_{5-6}=1.4507$ Å [4] compared with $R_{6-6}=1.40$ Å and $R_{5-6}=1.45$ Å from NMR experiments [23]. The optimized structures for spiroannelated quinone-type methanofullerenes are shown in Fig. 2 with molecule **1a** as an example. The quinone ring perpendicularly bisects the $C_{57}$–$C_{60}$ bond and forms a methanofullerene structure with the fullerene cage. Compound **1a** thus shows $C_{2v}$ symmetry, in accord with the 15 peaks observed [11, 12] for the fullerene moiety in the $^{13}C$ NMR spectrum, indicating the existence of two planes of symmetry. The symmetry of **1a** is consistent with Knight's calculation using the PM3 method [12]. In the $C_{60}$ part, there are 27 types of bonds, shown in Fig. 2a and Table 1. Their bond lengths may be compared with that of $C_{60}$.

**Table 1.** Bond lengths of the optimized structure for **1a** ($C_{2v}$)

| Kind of bond | Number of bond | Bond length | Bond index |
|---|---|---|---|
| 1 | 57–60 | 1.5340 | 0.8895 |
| 2 | 57–50, 57–52, 57–58, 60–59 | 1.4765 | 1.0080 |
| 3 | 50–40, 52–43, 58–56, 59–55 | 1.4446 | 1.1757 |
| 4 | 40–43, 56–55 | 1.4480 | 1.1270 |
| 5 | 50–49, 52–53, 58–51, 59–54 | 1.3916 | 1.4989 |
| 6 | 49–39, 53–44, 51–42, 54–45 | 1.4472 | 1.1540 |
| 7 | 49–51, 53–54 | 1.4620 | 1.0479 |
| 8 | 40–30, 43–33, 56–48, 55–47 | 1.4001 | 1.3669 |
| 9 | 39–32, 44–35, 42–32, 45–35 | 1.4504 | 1.1314 |
| 10 | 39–29, 44–34, 42–41, 45–46 | 1.3997 | 1.3730 |
| 11 | 29–30, 34–33, 41–48, 46–47 | 1.4453 | 1.1568 |
| 12 | 30–20, 33–23, 48–38, 47–37 | 1.4500 | 1.1309 |
| 13 | 20–23, 38–37 | 1.3980 | 1.3886 |
| 14 | 29–19, 34–24, 41–31, 46–36 | 1.4500 | 1.1334 |
| 15 | 32–22, 35–25 | 1.3971 | 1.3982 |
| 16 | 22–13, 25–15, 22–21, 25–26 | 1.4511 | 1.1293 |
| 17 | 13–19, 15–24, 21–31, 26–36 | 1.3983 | 1.3878 |
| 18 | 19–11, 24–14, 31–28, 36–27 | 1.4505 | 1.1335 |
| 19 | 11–20, 14–23, 28–38, 36–27 | 1.4507 | 1.1361 |
| 20 | 13–6, 15–8, 21–12, 26–16 | 1.4497 | 1.1399 |
| 21 | 6–12, 16–8 | 1.4520 | 1.1277 |
| 22 | 6–2, 16–8 | 1.3978 | 1.3890 |
| 23 | 6–2, 16–8 | 1.4500 | 1.1358 |
| 24 | 11–5, 7–14, 28–18, 27–17 | 1.3986 | 1.3870 |
| 25 | 5–7, 18–17 | 1.4500 | 1.1331 |
| 26 | 2–1, 3–1, 10–4, 9–4 | 1.4507 | 1.1320 |
| 27 | 1–4 | 1.3980 | 1.3928 |

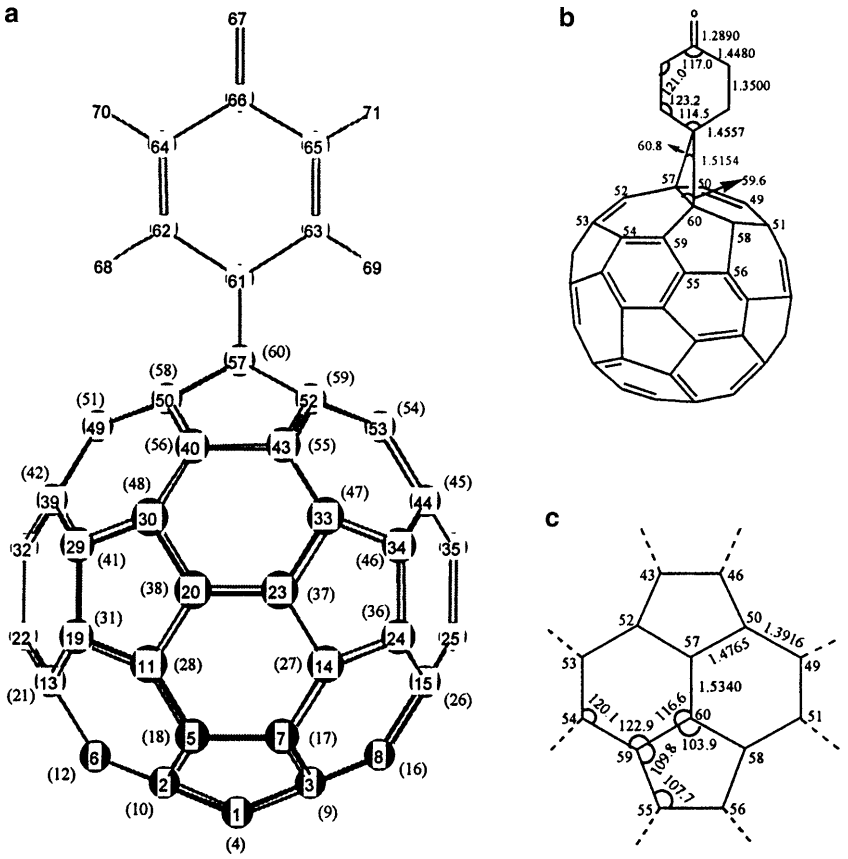


**Fig. 2.** Geometry structure of molecule **1a**. The *numbers* in *parentheses* are values for the reverse side of **1a**

The methano-bridged $C_{57}$–$C_{60}$ bond was calculated to have a length of 1.5340 Å, i.e., 0.0833 Å longer than the 6/6 junctions in $C_{60}$. The calculated value is in good agreement with the X-ray value of 1.553 Å for a methano-bridged dibenzohopyracylene [24, 25]. The lengthening of the $C_{57}$–$C_{60}$ bond is accompanied by the elongation of the four contiguous 5/6 bonds(1.4765 Å), which have $sp^3$–$sp^2$ character. The single bond, $C_{57}$–$C_{60}$, has a bond order of 0.8895 from the INDO/2 calculation. $C_{57}$–$C_{60}$ protrudes from the $C_{60}$ cage and causes all the surrounding C–C bonds to be stretched. In molecule **1a**, the bond indexes of the other bonds remain unchanged expect that $C_{57}$–$C_{60}$ changed from a double bond to a single bond. From bond $C_{57}$–$C_{60}$, the bond length of the other bond changed less and less as the bond from bond $C_{57}$–$C_{60}$ becomes longer and longer.

Figure 2b and 2c display the bond lengths and the angles of the pyracylene unit defined around the 6/6 junction where bridging occurs because the geometry of this unit undergoes the most noticeable change with respect to $C_{60}$. The bond angles surrounding the transannular $C_{57}$–$C_{60}$ bond present the largest deviations from the values of 120° and 108° found for the internal angles of hexagons and pentagons, respectively, in icosahedral $C_{60}$. The $C_{52}$–$C_{57}$–$C_{50}$ and $C_{59}$–$C_{60}$–$C_{58}$ angles are reduced to 103.9°.

The cyclohexadienone ring is joined to the $C_{57}$ and $C_{60}$ atoms by bonds of 1.5154 Å. This value is in good agreement with both the values of 1.521 Å reported using Knight's PM3 method [11] (shown in Table 2) and the values of 1.512 Å reported for a (diphenylmethano)

**Table 2.** Optimized geometric parameters with INDO and PM3 (bond distance: angstrom, bond angle: degree)

| Parameter | INDO/2 | PM3 |
|---|---|---|
| 57–70 | 1.5340 | 1.5480 |
| 57–50 | 1.4765 | 1.497 |
| 50–49 | 1.3916 | 1.375 |
| 49–51 | 1.4620 | 1.475 |
| 57–61 | 1.5154 | 1.521 |
| 61–63 | 1.4557 | 1.482 |
| 63–65 | 1.3500 | 1.335 |
| 65–66 | 1.4480 | 1.483 |
| 66–67 | 1.2890 | 1.218 |
| 59–60–58 | 103.9 | 104.0 |
| 55–59–60 | 109.8 | 109.2 |
| 59–55–56 | 107.7 | 108.2 |
| 54–59–60 | 122.9 | 122.3 |
| 53–54–59 | 120.1 | 120.8 |
| 59–60–57 | 116.6 | 116.6 |
| 57–61–50 | 60.8 | 61.6 |

fullerene [26]. The $C_{57}$–$C_{61}$–$C_{60}$ angle predicted for **1a** (60.8°) is very close to that obtained for the latter (61.6°). The geometry of the cyclohexadienone moiety is typical of a quinone-type structure with a large bond length alternation between single and double bonds (Fig. 2b).

The ZINDO-optimized geometries for the methanofullerene moiety in molecules **1b**, **1c**, **2**, **3** and **4** are analogous to that obtained for **1a** and show the same trends.

Steric interactions are most important for the anthraceno-fullerene molecules **3** and **4** owing to the short contacts between the aromatic peri hydrogens of the

anthracene unit and the $C_{60}$ ball. As depicted in Fig. 3 the INDO-optimized geometry calculated for **4** imposing a $C_{2v}$ and $C_s$ symmetry reveals that the folded $C_s$ structure is 36.32 kcal/mol more stable than the perpendicular $C_{2v}$ form. In the $C_{2v}$ case, the distance of the peri hydrogens to the 49, 51 and 53, 54 atoms is 1.7876 Å. To avoid these short contacts, the anthracene moiety is no longer perpendicular to the $C_{57}$–$C_{60}$ bond and its central ring is folded adopting a boat conformation. The resulting $C_s$ structure only shows two short contacts, at 2.5012 Å, between the two lower peri hydrogens and carbons $C_{59}$, $C_{52}$ and $C_{58}$, $C_{50}$. In this case, the folding of the anthracene moiety not only reduces the steric hindrance with the $C_{60}$ cage but also alleviates the nonbonding interactions that take place between the cyano groups and the upper peri hydrogens (Fig. 3). The "butterfly shape" adopted by the anthracene moiety in the $C_s$ structure can be defined in terms of the dihedral angles of the central quinone-type ring. The lower vertex $C_{61}$ is folded down with respect to the plane defined by the four central atoms $C_{62}$, $C_{63}$, $C_{64}$ and $C_{65}$ by an angle of 21.6° (see Fig. 2 for atom numbering). The upper vertex $C_{64}$ is folded by an angle of 40.6°. The lateral benzene rings preserve their planarity showing aromatic structures and form an angle of 154.1°. The folding of the anthracene has been previously discussed for 11, 11,12,12-tetracyano-9,10-anthraquinodimethane (TCAQ) derivatives, showing that theoretical ZINDO predictions are in accordance with X-ray observation [28] (Table 3). For TCAQ, the X-ray structure shows that the vertex carbon atom is folded down 30.4°; the lateral benzene rings also preserve their planarity and form an angle of 145°. Similar structures are found for **3**.

### 3.2 Electronic structure

On the basis of the geometry, we calculated the electronic structures of **1a** ($C_{66}H_4O$) as an example, which can be considered as two $\pi$ subsystems linked through a spiro atom $C_{61}$: $C_{60}$ and benzoquinone($C_6H_4O$). The MOs of $C_{60}$, $C_6H_4O$ and $C_{66}H_4O$ were calculated at the ZINDO level. Then the MO interaction diagram of $C_{60}+C_6H_4O \rightarrow C_{66}H_4O$ was plotted as shown in Fig. 4. The frontier orbitals of molecule **1a** are shown in Fig. 5. Figure 4 shows that the HOMO energy of $C_{60}$ is approximate to that of the addend, so the interaction between them takes place easily. The most immediate effect of methano-bridging substitution on the electronic structure of $C_{60}$ is the breaking of the orbital degeneracy associated with the icosahedral symmetry of the ball. Reducing the symmetry [$C_{60}(I_h) \rightarrow C_{60}$/benquinone($C_{2v}$)] splits the MO degeneracies and decreases the HOMO–LUMO energy gap. The five-fold degenerate $4h_u$ HOMO of $C_{60}$ calculated to be at −6.70 eV at the ZINDO level splits into five molecular orbitals ranging from −6.65 to −7.11 eV. Among these five orbitals, only the $32b_1$ HOMO sketched in Fig. 6 presents significant contributions

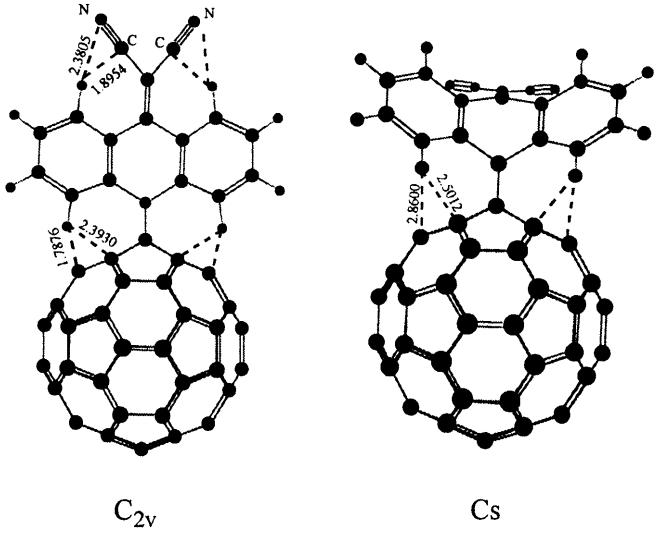


**Fig. 3.** Zerner's intermediate neglect of differential overlap optimized $C_{2v}$ and $C_s$ structures of molecule **4**. (See Fig. 2 for atom numbering.)

**Table 3.** Optimized geometric parameters for **4** and TCAQ

| Parameters | **4** INDO/2 | TCAQ X-ray |
|---|---|---|
| 66–65 | 1.4595 | 1.470 |
| 65–63 | 1.4148 | 1.412 |
| 66–67 | 1.3509 | 1.356 |
| 67–70 | 1.4209 | 1.435 |
| 70–71 | 1.2112 | 1.142 |
| 64–66–65 | 113.19 | 115.3 |
| 66–65–63 | 116.68 | 118.0 |
| 65–66–67 | 123.32 | 122.3 |
| 66–67–70 | 142.83 | 124.1 |
| 67–70–71 | 178.24 | 175.6 |

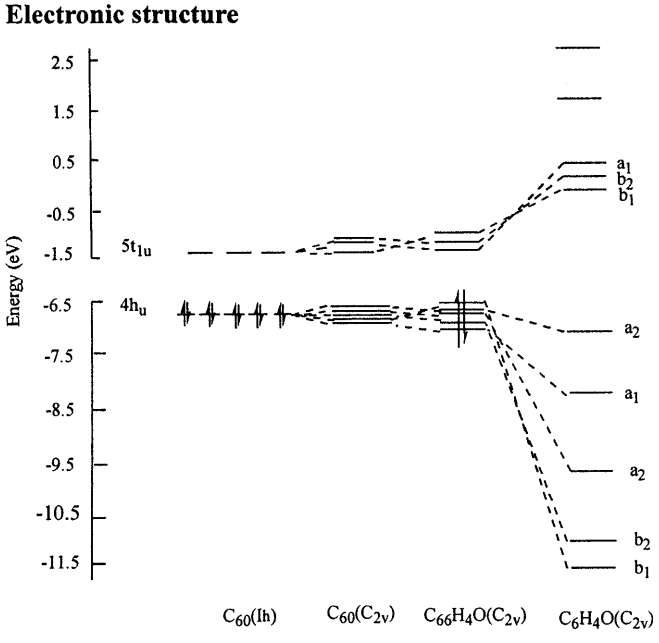


**Fig. 4.** The molecular orbital interaction diagram of $C_{60}+C_6H_4O \rightarrow C_{66}H_4O$

from the cyclohexadienone moiety. The orbital displays $2p$–$\pi$ bonding interactions for those bonds exhibiting a higher double-bond character in both the $C_{60}$ cage and the addend. The $\pi$ systems of both fragments further overlap giving rise to a through-space bonding interaction that has been previously named "periconjugation". Periconjugation differs from spiroconjugation in the relative orientations of the atomic orbitals (AOs) involved in the two interactions $\pi$ system. Even though a spiro atom also separates the $\pi$ system in the molecules involved, the mode of interaction of the corresponding $p_\pi$ orbitals is geometrically completely different from spiroconjugation, but they both belong to the lateral overlap. For spiroconjugation, there are four interacting $p_\pi$ orbitals. These orbitals are antisymmetric, corresponding to two perpendicular planes. However, for periconjugation, there are ten interacting $p_\pi$ orbitals. These orbitals are symmetric to their corresponding mirror planes. So more intense orbital interactions should be expected for periconjugation. This can be easily seen through looking at the relative orientations of the AOs involved (Fig. 6). The interaction of periconjugation for the HOMO of **1a** is small since the AO coefficients of the $C_{62}$ and $C_{64}$ atoms in the linear combination of AOs expansion are only 0.10.

We calculated the electronic structure of **2** as another representative example where periconjugation plays an important role in the HOMO. As depicted in Fig. 7, the AO contributions of the addend moiety to the HOMO are larger than those obtained for **1a** (cf. Figs. 6, 7) and give rise to an important through-space periconjugation effect. The key for the cyclohexadiene addend lies at −7.05 eV, i.e., 0.35 eV higher in energy than the HOMO of $C_{60}$ (−6.70 eV) and, therefore, strongly contributes to the HOMO of **2,** which appears at −6.79 eV. This is not the case for **1a** because the HOMO of the 1, 4-cyclohexadienone is calculated to be lower in energy at −7.33 eV and has a small contribution to the HOMO of **1a**.

We turn now to analyze the unoccupied orbitals of **1a**. Methano bridging produces a slight destabilization of the $5t_{1u}$ LUMO of $C_{60}$, which is split into three orbitals. The energy of the LUMO seems not to be affected by the size of the addend since the LUMO of the addend, calculated to be at −0.10 eV, lies very high in energy with respect to the LUMO of $C_{60}$ (−1.30 eV) and there is no effective overlap between the LUMOs of both fragments.

In addition, the Mulliken charge distribution of spiroannelated quinone-type methanofullerenes was calculated. The Mulliken charge on the $C_{60}$ part is 0.054. In free $C_{60}$, where all carbons are equivalent, the charge on each carbon is 0. It suggests that about 0.054 electron transfers from the $C_{60}$ part to the quinone part.

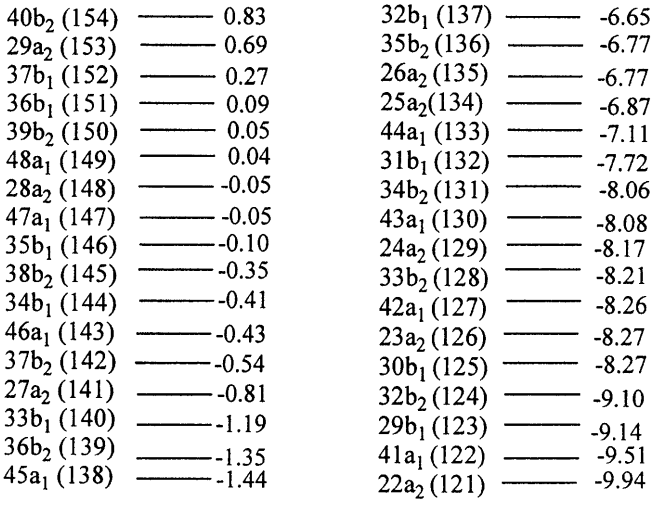


**Fig. 5.** The frontier orbital of molecules **1a** (unit: electron volts)

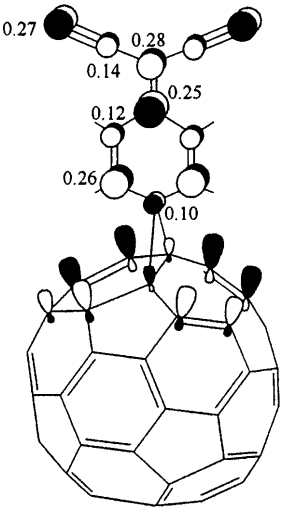


**Fig. 7.** The partial orbital of the HOMO for **2**

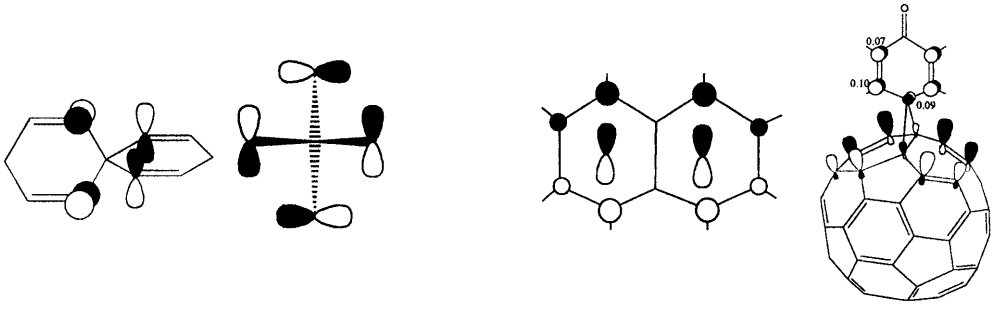


**Fig. 6.** Models of orbital interaction in spiroconjugation (*left*) and periconjugation (*right*)

### 3.3 UV–vis spectra

Using the INDO/single configuration interaction (SCI) method, the electronic spectra of spiroannelated quinone-type methanofullerenes were calculated. In the calculation, the active space of 17 occupied and 17 virtual orbitals with 289 single-electron excitation configurations and the ground state (total number is 290 configurations) is included. The calculated wavelength and oscillator strengths of the UV absorptions for molecules **1a**–**4** are listed in Tables 4 and 5 with the experimental values for comparison. The calculations are in good agreement with the experiments.

For these quinone-derived fullerenes, there are four strong absorption bands, at 211–217, 230–240, 247–249 and 272–329 nm. The former three absorptions are comparable with those of 213, 237 and 250 nm for $C_{60}$. The 211–217 and the 247–249 nm absorptions are also comparable with those of the 220–225 and 260–262 nm bands in the experiment, respectively. The UV–vis spectra of molecules **1a**–**4** have retained the main electronic feature of $C_{60}$. (In the MO analysis of molecule **1a**, we find that the 213.8-nm absorption comes from the electronic transfer on the $C_{60}$ three-dimensional conjugated sphere, which plays an important role in the NLO response.) The strong absorption bands near 272–329 nm are also comparable with the bands at 286–327 nm in the experiment. (In the MO analysis of molecule **1a**, we find that the 280.5-nm absorption comes from mixing of benzoquinone with $C_{60}$).

Owing to the interaction between the $C_{60}$ and quinone addends, the weak absorptions over 410 nm become significant for these spiroannelated quinone-type methanofullerenes. These absorptions do not appear in free $C_{60}$ and can be considered as characteristic absorptions of spiroannelated quinone-type methanofullerenes. The calculated wavelengths and oscillator strengths, which are larger than 0.001, are listed in Table 5 with some experimental values for comparison. The ZINDO-calculated characteristic absorptions are in good agreement with those of experiments. Recently, the relatively strong characteristic absorption at about 440 nm has been observed in several experiments.

In addition, reducing the symmetry [$C_{60}(I_h)\rightarrow 1$, $2(C_{2v})$ and 3, $4(C_s)$] splits the MO degeneracies. In $C_{2v}$ symmetry, only transitions $a_1\rightarrow a_2$ and $b_1\rightarrow b_2$ are symmetry-forbidden, while in $C_s$ symmetry all MOs are nondegenerate and all transitions ($a'\rightarrow a'$ or $a''\rightarrow a''$) are symmetry-allowed.

### 3.4 NLO property

On the basis of having predicted the electronic spectra correctly, we proceeded to calculate the nonlinear second-order optical susceptibility $\beta_{ijk}$ and $\beta_\mu$ by using the ZINDO–SOS method.

In the SOS expression (Eq. 2) for $\beta$, the summation is over the complete sets of eigen states $|n>$, $|m>$ and $|q>$ of the unperturbed system. They have to be truncated in the practical calculation [7, 30] for feasibility. In Eq. (2), the dominator of each term includes $\omega_{ng}$, $\omega_{n'g}$. When $n$ and $n'$ increase, the energy differences between the ground state and the excited states will increase, i.e., the denominator will increase more and more. This means the contribution for $\beta$ will become less important when $n$ and $n'$ reach a certain value. Li et al. [4] demonstrated that 197 excited states were found to be sufficient for effective convergence for $C_{60}$. However, the spiroannelated quinone-type methanofullerenes considered are more complicated than $C_{60}$, only 197 excited states were insufficient for effective convergence. Thus, 290 configurations were included in the calculations of $\beta$, which was sufficient for effective convergence. The plot of $\beta_\mu$ against excited state number, $N$, is shown in Fig. 8 with molecule **1a** as an example. The converged $\beta_\mu$ is simplified as $\beta$ (listed in Table 6), where $\beta_0$ corresponds to $\omega = 0$. The values of $\beta$ relate to $\omega$, the laser field frequency. $\omega$ is taken as 1.064 $\mu$m. As we expected, the inclusion of quinone addends makes the derived fullerenes possess a relatively large $\beta$.

The $\beta$ accumulations with up to 290 excited states with **1a** are shown in Fig. 8 as an example. The 1st, 104th and 203rd excited states are the most important ones that significantly contribute to the second-order susceptibilities. Similar trends also have been found in molecules **1b, 1c, 2**–**4**.

The lowest-energy absorption, at 580.9 nm, is induced by the symmetry-allowed electron transition from the HOMO ($32b_1$) to the LUMO ($45a_1$). The component for both the HOMO and the LUMO of **1a** concentrates on the $C_{60}$ moiety. The electron transition can be assigned as the charge transfer within the $C_{60}$ three-dimensional conjugated sphere. We calculated $\Delta\mu$, the difference in the

**Table 4.** Strong absorption of spiroannelated quinone-type methanofullerenes ($\lambda$: wavelength; $f$: oscillator strength)

| | **1a** | | **1b** | | **1c** | | **2** | | **3** | | **4** | | $C_{60}$ | |
|---|---|---|---|---|---|---|---|---|---|---|---|---|---|---|
| | $\lambda$/nm | $f$ | $\lambda$/nm | $f$ | $\lambda$/nm | $f$ | $\lambda$/nm | $f$ | $\lambda$/nm | $f$ | $\lambda$/nm | $f$ | $\lambda$/nm | $f$ |
| Calculated | 213.8 | 4.7542 | 211.1 | 4.8853 | 211.9 | 4.9588 | 212.3 | 5.4462 | 216.5 | 4.5243 | 215.6 | 4.8074 | 213.3 [4] | 27.87 |
| | 230.2 | 1.5030 | 235.7 | 1.0976 | 234.1 | 1.0252 | 234.0 | 1.3644 | 236.6 | 1.2659 | 239.6 | 1.1207 | 236.1 | 3.75 |
| | 247.4 | 1.1036 | 247.8 | 1.0965 | 247.9 | 1.1682 | 247.3 | 1.2425 | 254.1 | 0.6553 | 248.7 | 1.2098 | 250.4 | 3.41 |
| | 280.5 | 2.0361 | 276.4 | 1.9521 | 272.1 | 1.9773 | 328.5 | 2.0788 | 276.3 | 1.0663 | 306.8 | 1.1177 | | |
| Experiment | 225 [12] | 222 [12] | 220 [12] | | | | | | | | | | 211 [29] | Strong |
| | 262 | 260 | 260 | | | | | | | | | | 227 | Shoulder |
| | 327 | 315 | 315 | | | | | | 286 [12] | | 330 [11] | | 256 | Strong |

**Table 5.** Special absorption band of spiroannelated quinone-type methanofullerenes ($\lambda$: wavelength; $f$: oscillator strength)

| | **1a** | | **1b** | | **1c** | | **2** | | **3** | | **4** | | $C_{60cal}$ | |
|---|---|---|---|---|---|---|---|---|---|---|---|---|---|---|
| | $\lambda$/nm | $f$ | $\lambda$/nm | $f$ | $\lambda$/nm | $f$ | $\lambda$/nm | $f$ | $\lambda$/nm | $f$ | $\lambda$/nm | $f$ | $\lambda$/nm | $f$ |
| Calculated | 580.9 | 0.0039 | 582.1 | 0.0039 | 581.4 | 0.0039 | 580.1 | 0.0039 | 602.1 | 0.0080 | 600.1 | 0.0076 | 558.3 | 0.00 [4] |
| | 495.4 | 0.0036 | 518.8 | 0.0018 | 519.9 | 0.0038 | 520.3 | 0.0013 | 525.9 | 0.0038 | 524.0 | 0.0064 | 550.7 | 0.00 |
| | 463.5 | 0.0019 | 495.6 | 0.0033 | 495.6 | 0.0035 | 494.8 | 0.0034 | 491.4 | 0.0055 | 497.2 | 0.0033 | 537.6 | 0.00 |
| | 443.2 | 0.0106 | 443.6 | 0.0042 | 442.1 | 0.0085 | 463.4 | 0.0097 | 453.2 | 0.0086 | 446.9 | 0.0082 | 473.2 | 0.00 |
| | 441.5 | 0.0054 | 441.7 | 0.0119 | 441.3 | 0.0046 | 443.2 | 0.0066 | 441.3 | 0.0107 | 443.0 | 0.0131 | | |
| | 434.6 | 0.0026 | 435.1 | 0.0029 | 435.2 | 0.0035 | 441.1 | 0.0094 | 436.3 | 0.0032 | 439.2 | 0.0047 | | |
| | | | | | | | 434.8 | 0.0105 | 427.4 | 0.0016 | 434.2 | 0.0061 | | |
| Experiment | 440 [12] | | 440, 500 [12] | | | | 436, 496, 696 [12] | | 434, 492, 694 [11] | | | | | |

dipole moments between the ground state and the first excited state. The calculated $\Delta\mu$ is 2.8 D. Sequentially, the contribution of the first excited state to $\beta$ is calculated by using a two-level approximation:

$$\beta_\mu = \frac{3e^2\hbar^2}{2m}\frac{Wf\Delta\mu}{\left[W^2-(2\hbar\omega)^2\right]\left[W^2-(\hbar\omega)^2\right]} \quad .$$

Here $\omega$ is the frequency of the laser field and $W = \hbar\omega_{ng}$ is the transition energy from the ground state to the excited state; $f$ is the oscillator strength of the transition and $\Delta\mu$ is the difference in the dipole moments between the excited state and the ground state. The calculated contribution to the $\beta$ value is $12.4 \times 10^{-30}$ esu.

The 104th excited state induces a medium absorption at 280.5 nm of **1a**. The absorption comes from mixing of the electron transitions from HOMO – 5 to LUMO + 3 and from HOMO to LUMO + 9 orbitals. In the HOMO – 5 and LUMO + 3 orbitals, the component on the $C_{60}$ part is dominant. Therefore, such a kind of transition can be assigned as electron transfer on the $C_{60}$ three-dimensional conjugated sphere. In the HOMO and the LUMO + 9, the components concentrate on the $C_{60}$ part and the cyclohexadienone ring, respectively (shown in Fig. 9). The electronic transition from the HOMO to the LUMO + 9 orbital can be assigned as electronic transfer from the $C_{60}$ part to the benzoquinone part. The mixing of these transitions is regarded as the source of the NLO susceptibility. Figure 8 indicates that the contribution of the 104th excited state to $\beta$ is $24.08 \times 10^{-30}$ esu ($\beta_{104} - \beta_{103} = 60.99 - 36.91$, $\beta_{103}$, $\beta_{104}$ correspond to the accumulated $\beta$ of 103 excited states and that of 104 excited states).

The 203rd excited state that induces absorption at 213.8 nm comes from the mixing of the electron transition from HOMO–14 to LUMO + 1, HOMO-13 to LUMO + 2, HOMO–11 to LUMO + 8, HOMO–10 to LUMO + 10 and HOMO–9 to LUMO + 14. The component on the $C_{60}$ part is dominant for these orbitals. Therefore, the five electronic transitions can all be assigned as electronic transfer within the $C_{60}$ three-dimensional conjugated sphere. The mixing of these transitions is regarded as the source of the NLO susceptibility. In the molecules involved, these high-energy excited state absorptions have larger oscillator strengths than the others. The contribution of the 203rd excited state to the $\beta$ value is $32.16 \times 10^{-30}$ esu ($\beta_{203}$–$\beta_{202} = 157.77$–$125.61$).

Compared with the traditional fullerene derivatives reported, the calculated $\beta$ values of spiroannelated quinone-type methanofullerenes are unusually large [7, 9]. The large NLO response may be attributed to periconjugation between the two subsystems, which results in the strong through-space orbital interaction between the two subsystems and transmits the electron-withdrawing effect of the carbonyl group of the addend. As has been mentioned, periconjugation differs from spiroconjugation in the relative orientations of the AOs involved in the two interacting $\pi$ systems (Fig. 6) and induced more intense orbital interaction than that of spiroconjugation. Recently, interest has increased tremendously in the

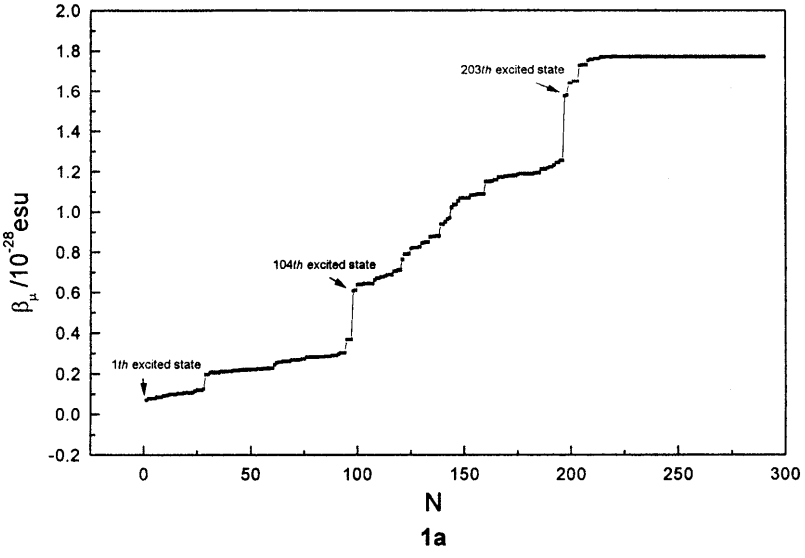


**Fig. 8.** $\beta$ values plotted against numbers of excited states for molecule **1a**

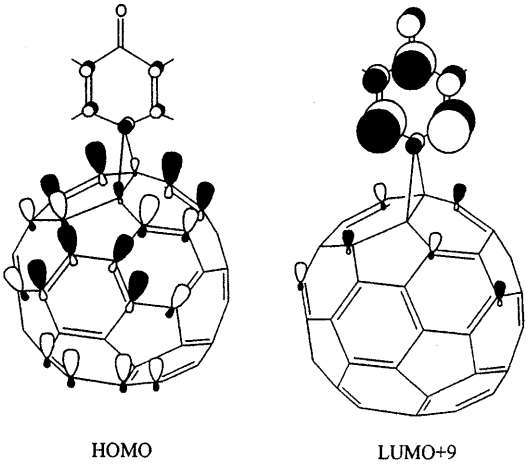


**Fig. 9.** Atomic orbital composition of the HOMO and the LUMO + 9 of molecule 1a

NLO properties of the spiroconjugated compounds [32, 33, 34, 35]. We have reported some investigations of the spiroconjugation effect on the NLO properties [35, 36], which show that the spiroconjugated compounds have medium second-order NLO susceptibility. As was expected, the periconjugated compounds have large second-order NLO susceptibilities. To further explore the effect of periconjugation on $\beta$, we designed molecule **5** [11], with a saturated bond in the quinone moiety, and molecule **6** [6], with a different spacer between $C_{60}$ and quinone, and calculated their UV–vis spectra and $\beta$ using the ZINDO–SOS method. The calculated $\beta$ values of molecule **5** and **6** are shown in Table 7 with that of molecule **1a** for comparision.

The calculated $\beta$ of molecule **1a** is larger than those of molecules **5** and **6**. The enhancement may be attributed to periconjugative interaction, which transmits the electron-withdrawing effect of the carbonyl group of the addend. However, such interaction does not exist in molecules **5** and **6**. For molecule **5**, the bonds of the addend are saturated; thus, the electron-withdrawing effect is more poorly transmitted. For molecule **6**, it is lack of conjugation between the two subsystems.

**Table 6.** $\beta$ and $\beta_0$ for spiroannelated quinone-type methanofullerenes

| Molecule | $\mu$/D | $\beta_{cal}/10^{-30}$ esu ($\omega$ = 1.064 $\mu$m) | $\beta_{0cal}/10^{-30}$ esu | $\beta_{exp}/10^{-30}$ esu |
|---|---|---|---|---|
| **1a** | 7.17 | 177.726 | 124.284 | |
| **1b** | 5.77 | 139.927 | 103.098 | |
| **1c** | 5.79 | 132.823 | 103.519 | |
| **2** | 10.07 | 289.494 | 222.706 | |
| **3** ($C_{2v}$) | 5.01 | 134.497 | 100.324 | |
| **3** ($C_s$) | 4.74 | 94.024 | 78.664 | |
| **4** ($C_{2v}$) | 9.39 | 307.829 | 307.829 | |
| **4** ($C_s$) | 8.33 | 192.277 | 143.506 | |
| $C_{60}$ | 0 | 0 | 0 | |
| $C_{60}$/AN | | 32.17 [7] | 20.42 [7] | 67 ± 20 [31] |

In addition, we calculated the $\beta$ values of **3** and **4** with $C_{2v}$ and $C_s$ symmetry. Figure 3 shows that the distance of the peri hydrogens to the 49, 51 and 53, 54 atoms is 1.7876 Å in the $C_{2v}$ case for molecule **4**; the calculated results show that its HOMO orbital has intense orbital interaction "periconjugation"; however, in $C_s$ symmetry, owing to central ring of the anthracene moiety being folded up, the resulting $C_s$ structure only shows two short contacts, at 2.5012 Å, between the two lower peri hydrogens and carbons $C_{59}$, $C_{52}$ and $C_{58}$, $C_{50}$. Therefore, the $C_s$ structure has very little "periconjugation" interaction. The calculated $\beta$ with $C_{2v}$ and $C_s$ for molecules **3** and **4** are also listed in Table 6. The $\beta$ of **3** is $134.0 \times 10^{-30}$ esu and that of **4** is $307.83 \times 10^{-30}$ esu for $C_{2v}$ symmetry; however, the $\beta$ of **3** is $94.02 \times 10^{-30}$ esu and that of **4** is $192.28 \times 10^{-30}$ esu for $C_s$ symmetry. The small $\beta$ of the $C_s$ structure is attributed to the loss of periconjugation. Thus, it can be concluded that the periconjugation effect plays an important role in the large $\beta$. Molecules **2** and **4** (introduced strong acceptor – dicyanovinyl group) have stronger periconjugation than **1a** and **3**; their $\beta$ values are much larger than those of the

**Table 7.** The UV–vis spectra and $\beta$ ($10^{-30}$ esu) of molecules **1a**, **5** and **6**

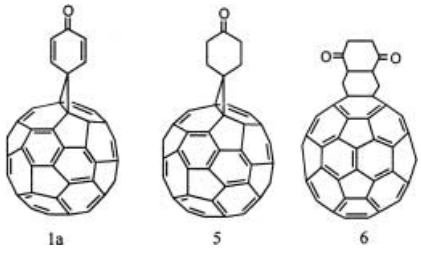

| Molecule | $\lambda_{cal}$ | $\lambda_{exp}$ | $\mu$ | $\beta$ | $\beta_0$ |
|---|---|---|---|---|---|
| **1a** | | | 7.17 | 177.726 | 124.284 |
| **5** | 593.8, 435.1, 251.7, 237.5, 212.9 | 432, 255 | 1.72 | 35.167 | 26.528 |
| **6** | 582.1, 442.1, 235.3, 214.0 | | 3.74 | 58.523 | 45.155 |

latter. Except for the effect of the electron-withdrawing group, we attribute these large enhancements to the effect of periconjugation.

The effect of the electron donor/acceptor is also considered. Introducing the electron-donating group, $-CH_3$ (**1b**) and $-t$-$C_4H_9$ (**1c**) into the addend of **1a** is not favorable for the electron transfer from $C_{60}$ to benquinone. The dipole moment decreases. The $\beta$ values of **1b** and **1c** become smaller compared with that of **1a**. In contract, on introducing a strong electron-withdrawing group – dicyanovinyl group – into the addends of **1a** and **3**, the dipole moments of **2** and **4** increase. The $\beta$ values are greatly increased (Table 6).

Additionally, it should be noted that the NLO properties of the quinone-derived fullerenes are different from those of the traditional push–pull conjugated organic molecules. For the traditional organic molecules, the first excited state (the lowest-energy excited state), corresponding to the electronic transition from the HOMO to the LUMO, is mostly taken as the most important excited state, which dominates the second-order NLO response. However, for the quinone-derived fullerenes, besides the first excited state, some high-energy excited states, which induce the strong absorptions in high-lying excited bands, also play important roles in the NLO responses. In principle, a configuration interaction scheme limited to singly excited configurations might not suffice to describe the high-lying excited states. However, the necessity of including all the states that might be resonant in second harmonic generation would make the number of electronic states in the SOS calculation too large to handle [37]. In the light of previous work [4, 37] which showed that, for fullerenes, the inclusion of doubly excited configurations does not alter the results obtained only with the single excitations we limit our configuration interaction to singles. It is the ability of the calculations to simulate the experimental results that is called upon to evaluate their accuracy.

## 4 Conclusion

ZINDO calculations were carried out to investigate the geometries, electronic structures, UV–vis spectra and charge-transfer interactions and to evaluate the second-order nonlinear susceptibilities for a series of spiroannelated quinone-type methanofullerenes. The calculated values of $\beta$ are large (130–300 $\times$ $10^{-30}$ esu), which shows a dramatic increase when the spiroannelated quinone-type groups are introduced. The NLO response can mainly be attributed to the result of electron transfer on the $C_{60}$ three-dimensional conjugated sphere and to the electron transfer from $C_{60}$ to addends. These spiroannelated quinone-type methanofullerenes will hopeful be a useful type of nonlinear second-order optical materials.

Spiroannelated quinone-type methanofullerenes were stronger electronic acceptors compared with $C_{60}$. Further work devoted to introducing strong donors into quinone-type fullerenes, which result in stronger charge transfer and, therefore, larger $\beta$ values is planned.

*Acknowledgements*. This work was supported by the National Natural Science Foundation of China.

## References

1. Kroto HW, Heath JR, Obrien SC, Curl RF, Smalley RE (1985) Nature 318: 162
2. Fowler PW, Woolrich J (1986) Chem Phys Lett 127: 78
3. Larsson S, Volosov A, Rosen A (1987) Chem Phys Lett 137: 501
4. Li J, Feng JK, Sun JZ (1993) Chem Phys Lett 203: 560
5. Krätschmer W, Lamb LD, Fostiropoulos K, Huffman DR (1990) Nature 347: 354
6. Lyoda M, Sultana F, Sasaki S, Yoshids MJ (1994) J Chem Soc Chem Commun 1929
7. Li J, Feng JK, Sun CC (1994) J Phys Chem 98: 8636
8. Matsuzawa N, Dixon DA, Fukunaga T (1992) J Phys Chem 96: 7594
9. Feng JK, Fu W, Cui M, Su ZM, Ren AM (2000) J Acta Chim Sin 58: 1112
10. Zhang SQ, Feng JK, Ren AM, Fu W, Li YX (2000) J Acta Chim Sin 58: 1582
11. Knight B, Martån N, Ohno T, Ortå E, Rovira C, Veclana J, Gancedo JV, Viruela P, Viruela R, Wudl F (1997) J Am Chem Soc 119: 9871
12. Ohno T, Matån N, Knight B, Wudl F, Suzoktå T, Yu HN (1996) J Org Chem 61: 1306
13. Eiermannn M, Haddon R, Knight B, Li QC, Maggini M, Martån N, Ohno Tproto M, Suzuki T, Wudl F (1995) Angew Chem Int Ed Engl 34: 1591
14. Ridley J, Zerner MC (1973) Theor Chim Acta 32: 111
15. Orr BJ, Ward TF (1971) Mol Phys 20: 513
16. Bishop DM (1994) Adv Quantum Chem 25: 1

17. Bella SD, Fragala IL, Ratner MA, Marks TJ (1993) J Am Chem Soc 115: 682
18. Ulman A, Willand CS, Kohler W, Tobello DR, Williams DJ, Handley L (1990) J Am Chem Soc 112: 7083
19. Feng JK, Gao XS, Sun CC (1990) Chin Sci Bull 35: 2022
20. Gao XL, Feng JK, Sun CC (1992) Int J Quantum Chem 42: 1747
21. Li J, Feng JK, Sun CC (1994) Int J Quantum Chem 52: 673
22. Feng JK, Gao XL, Sun CC (1992) J Acta Chim Sin 50: 111
23. Yannoni CS, Bernier PP, Bethune DS, Meijer G, Salem JR (1991) J Am Chem Soc 113: 3190
24. Anderson HL, Boudon C, Diederich F, Gisselbrecht JP, Gross M, Seiler P (1994) Angew Chem Int Ed Engl 33: 1628
25. Vogel E (1993) Pure Appl Chem 65: 143
26. Osterodt J, Nieger M, Vögtle F (1994) J Chem Soc Chem Commun 1607
27. Bondi A (1964) J Phys Chem 68: 441
28. Ortå E, Viruela R, Viruela PM (1996) J Phys Chem 100: 6138
29. Ajir H, Alvarez MM, Anz SJ, Beek RD, Diederich F, Fostiropoulos K, Huffman DR, Kratschmer W, Rubin Y, Schriver KE, Sencharma D, Whetten RL (1990) J Phys Chem 94: 8630
30. Kanis DR, Ratner MA, Marks TJ (1992) J Am Chem Soc 114: 10338
31. Wang Y, Cheng L (1992) J Phys Chem 96: 1530
32. Abe J, Shirai Y (1997) J Phys Chem B 101: 145
33. Abe J, Shirai Y (1997) J Phys Chem A 101: 1
34. Kim SY, Lee M, Boo BH (1998) J Chem Phys 109: 12593
35. Feng JK, Sun XY, Ren AM, Yu KQ, Sun CC (1999) J Mol Struct 489: 247
36. Sun XY, Feng JK, Ren AM, Su ZM, FuW, Jin HW (2000) Chem J Chin Univ 21: 1080
37. Fanti M, Orlandi G, Zerbetto F (1995) J Am Chem Soc 117: 6101